CONTRIBUTION OF FIN TO SIDEFORCE, YAWING MOMENT AND ROLLING MOMENT DERIVATIVES DUE TO RATE OF ROLL, $(Y_p)_F$, $(N_p)_F$, $(L_p)_F$, IN THE PRESENCE OF BODY, WING AND TAILPLANE

1. NOTATION AND UNITS (see Sketch 1.1)

The derivative notation used is that proposed in ARC R&M 3562 (Hopkin, 1970) and described in Item No. 86021. Coefficients and aeronormalised derivatives are evaluated in aerodynamic body axes with origin at the aircraft centre of gravity and with the wing span as the characteristic length. The derivatives Y_p, N_p and L_p are often written as C_{Yp}, C_{np} and C_{lp} in other systems of notation, but attention must be paid to the reference dimensions used. In particular, in forming C_{Yp}, C_{np} and C_{lp} differentiation of C_Y, C_n and C_l may be carried out with respect to $pb/2V$ not pb/V as implied in the Hopkin system. It is also to be noted that a constant datum value of V is employed by Hopkin.

		SI	*British*
A_F	effective aspect ratio of fin, $2h_F^2/S_F$		
A_T	tailplane aspect ratio, b_T^2/S_T		
A_W	wing aspect ratio, b^2/S_W		
b	wing span	m	ft
b_T	tailplane span	m	ft
C_l	rolling moment coefficient, $\mathscr{L}/\frac{1}{2}\rho V^2 S_W b$		
C_n	yawing moment coefficient, $\mathscr{N}/\frac{1}{2}\rho V^2 S_W b$		
C_Y	sideforce coefficient, $Y/\frac{1}{2}\rho V^2 S_W$		
c_{0T}	tailplane centre-line chord (in plane of symmetry)	m	ft
c_{rF}	fin root chord, see Sketch 1.1	m	ft
c_{tF}	fin tip chord, see Sketch 1.1	m	ft
h_F	height of fin, measured from fin root chord in direction normal to longitudinal body axis, see Sketch 1.1	m	ft
K_1, K_2, K_3	factors used in estimating $(Y_p)_F$, see Sections 3.1 and 3.2		
$\mathscr{L}$	rolling moment	N m	lbf ft
L_p	rolling moment derivative due to rate of roll, $L_p = (\partial\mathscr{L}/\partial p)/\frac{1}{2}\rho V S_W b^2$		
$(L_p)_F$	fin contribution to L_p in presence of body, wing and tailplane		

Issued April 1983
With Amendment A, March 1985

$(L_p)_T$	tailplane contribution to L_p in presence of body, wing and fin		
$\overline{l}_F^*$	distance of centre of pressure position of fin sideforce due to rate of roll, measured aft from centre of gravity position and parallel to longitudinal body axis, see Sections 3.1 and 3.2	m	ft
M	free-stream Mach number		
m_F	distance of fin root quarter-chord station aft of centre of gravity position, measured parallel to aircraft longitudinal body axis, see Sketch 1.1	m	ft
$\mathcal{N}$	yawing moment	N m	lbf ft
N_p	yawing moment derivative due to rate of roll, $N_p = (\partial\mathcal{N}/\partial p)/\frac{1}{2}\rho V S_W b^2$		
$(N_p)_F$	fin contribution to N_p in presence of body, wing and tailplane		
p	roll rate	radian/s	radian/s
S_F	fin area between fin root and tip chords, $h_F(c_{rF}+c_{tF})/2$, see Sketch 1.1	m^2	ft^2
S_T	tailplane planform area	m^2	ft^2
S_W	wing planform (reference) area	m^2	ft^2
V	velocity of aircraft relative to air	m/s	ft/s
v	sideslip velocity	m/s	ft/s
Y	sideforce	N	lbf
Y_p	sideforce derivative due to rate of roll, $Y_p = (\partial Y/\partial p)/\frac{1}{2}\rho V S_W b$		
$(Y_p)_F$	fin contribution to Y_p in presence of body, wing and tailplane		
z_{crf}	height of fin root chord, measured from longitudinal body axis in direction normal to longitudinal body axis, see Sketch 1.1	m	ft
$\overline{z}_F^*$	distance of centre of pressure position of fin sideforce due to rate of roll, measured above and normal to longitudinal body axis, see Sections 3.1 and 3.2	m	ft
z_T	height of intersection of fin-mounted tailplane with fin, measured from fin root chord in direction normal to longitudinal body axis, see Sketch 1.1	m	ft
α	angle of attack	radian	radian
β	angle of sideslip, $\sin^{-1}(v/V)$	radian	radian

β_F	angle of sideslip at fin	radian	radian
$\Lambda_{¼F}$	fin quarter-chord sweep angle	degree	degree
$\Lambda_{¼T}$	tailplane quarter-chord sweep angle	degree	degree
$\Lambda_{¼W}$	wing quarter-chord sweep angle	degree	degree
λ	ratio of wing tip chord to wing centre-line chord		
λ_F	ratio of fin tip chord to fin root chord		
λ_T	ratio of tailplane tip chord to tailplane centre-line chord		
ρ	density of air	kg/m^3	$slug/ft^3$
$\bar{\sigma}$	sidewash angle at fin due to rolling flight, positive when it decreases sideslip angle at fin, $\beta_F = \beta - \bar{\sigma}$	radian	radian
$\bar{\sigma}_W$	mean contribution to $\bar{\sigma}$ due to wing, see Section 3.3	radian	radian
$\bar{\sigma}_\alpha$	effective change in $\bar{\sigma}$ due to change in α and movement of fin relative to roll axis, see Section 3.4	radian	radian

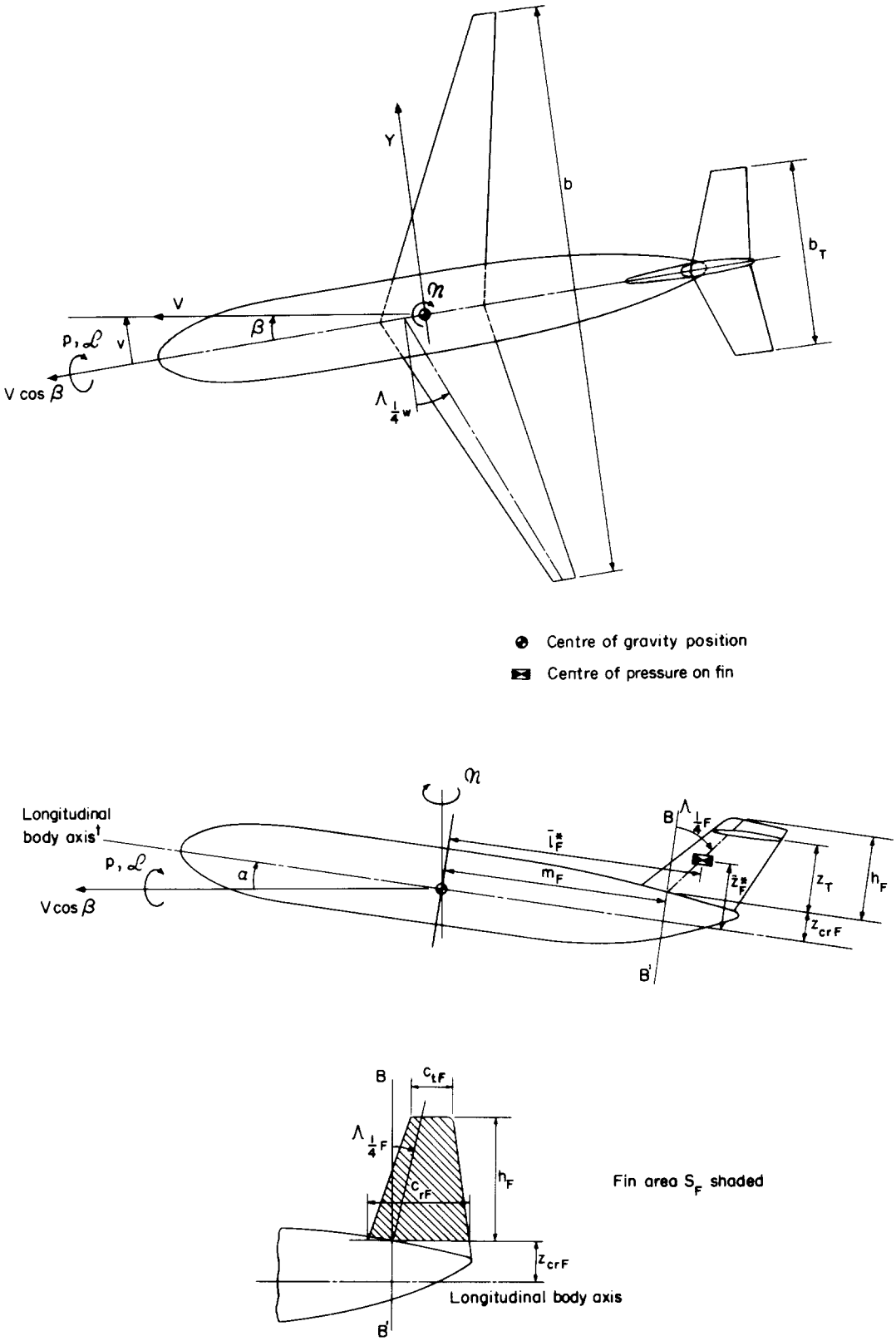

Sketch 1.1 Body, wing and fin geometries

† The longitudinal body axis is a reference axis, fixed in the body in the plane of symmetry and passing through the centre of gravity position. The exact direction of the axis in the plane of symmetry is conventionally determined by considerations of mid-body geometry, the axis being taken parallel to some convenient 'horizontal' datum.

2. INTRODUCTION

This Item gives a method for calculating $(Y_p)_F$, $(N_p)_F$, and $(L_p)_F$, the contributions of the vertical stabilising fin of an aircraft to the sideforce, yawing moment and rolling moment derivatives due to rate of roll. The method is applicable for subsonic flight speeds when the flow over the aircraft is wholly subsonic and fully attached. The tail assemblies covered are those where a single fin is located on top of the aircraft rear body and in the plane of symmetry, with a tailplane, if present, mounted either on the fin itself or on the rear body. The aircraft is assumed to be in the 'clean' configuration with no flaps or slats deployed. The method is semi-empirical; it makes use of the theoretical calculations performed for isolated fin-tailplane arrangements at zero angle of attack that are reported in Derivations 10, 16 and 20, and applies corrections to allow for the presence of the wing and body and for angle of attack variations. These corrections are made in terms of the mean sidewash occurring at the fin in rolling flight, as suggested in Derivations 3 and 5, with the magnitudes of the corrections being deduced from comparisons with the wind-tunnel test results given in Derivations 1 to 4, 6 to 9, 11 to 15, 17 to 19, 21 and 22. A method for calculating $(L_p)_T$, the contribution of the tailplane to L_p, is also included in the Item.

The method is described in detail in Section 3 (see Section 3.1 for $(Y_p)_F$, $(N_p)_F$, and $(L_p)_F$, and Section 3.1.2 for $(L_p)_T$). The accuracy and applicability are assessed in Section 4 on the basis of comparisons with wind-tunnel data. The Derivation and References are given in Section 5 and a worked example which illustrates the agreement between prediction and experiment is given in Section 6.

2.1 General Behaviour of Derivatives

As an introduction to the fin contributions to the roll rate derivatives, Sketch 2.1 shows the total (experimental) values of Y_p, N_p and L_p and the (experimental) fin contributions to these derivatives for a wind-tunnel model tested both with and without a wing (Derivation 3). The sketch demonstrates the important influence of the wing on the fin contributions, the interference being sufficient to change the sign of the derivatives at low angles of attack. Note also that the fin contribution to L_p is only a small part of the total aircraft value, and so it is subject to more uncertainty than the other two derivatives when deduced from fin-on and fin-off model tests. The method in this Item has therefore concentrated on predicting $(N_p)_F$, this being more important than $(Y_p)_F$ in stability calculations. (The substantial non-linear variation with α of the wing-on derivatives is attributable to the contribution of the wing planform, as described in Item No. 81014, Reference 25.)

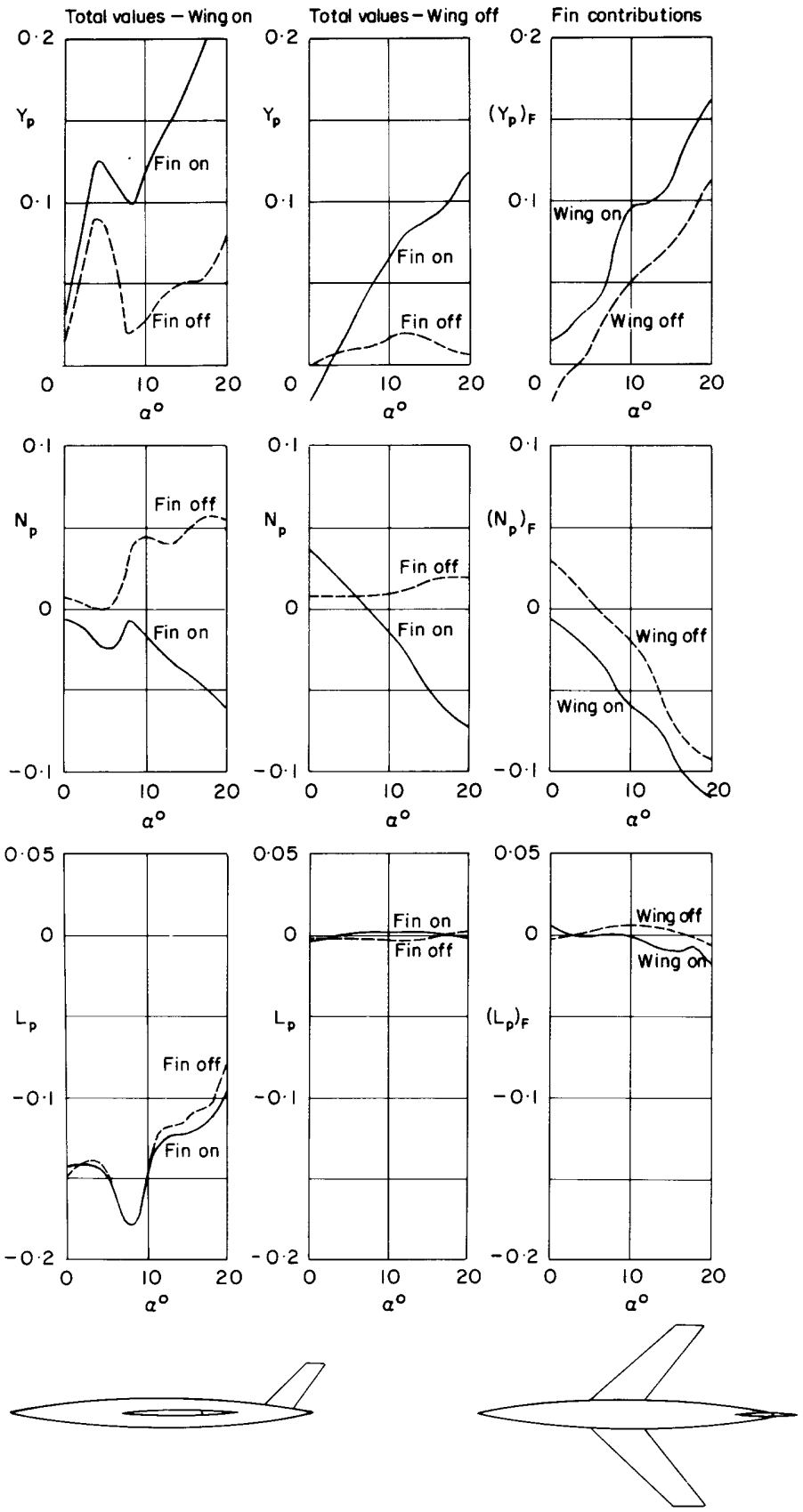

Sketch 2.1 Typical variations of roll rate derivatives (Derivation 3)

3. METHOD

3.1 General Equations

The equations required for predicting the fin contributions to the roll-rate lateral stability derivatives are set out in this section, with Section 3.1.1 discussing variations with Mach number and Section 3.1.2 giving the method for predicting the tailplane contribution $(L_p)_T$. Sections 3.2 to 3.4 describe how the equations have been developed.

The fin contributions are:

$$(Y_p)_F = -(K_1 + K_2K_3)\frac{S_F h_F}{S_W b}\left\{\frac{(\overline{z_F^*}\cos\alpha - \overline{l_F^*}\sin\alpha)/b - \partial\bar{\sigma}_W/\partial(pb/V) - \partial\bar{\sigma}_\alpha/\partial(pb/V)}{(\overline{z_F^*} - z_{crF})/b}\right\}, \tag{3.1}$$

$$(N_p)_F = -(Y_p)_F(\overline{l_F^*}\cos\alpha + \overline{z_F^*}\sin\alpha)/b\,, \tag{3.2}$$

and

$$(L_p)_F = (Y_p)_F(\overline{z_F^*}\cos\alpha - \overline{l_F^*}\sin\alpha)/b\,, \tag{3.3}$$

where $\overline{z_F^*}$ and $\overline{l_F^*}$ are the coordinates of the centre of pressure position of the fin damping force, in directions normal and parallel to the body longitudinal axis, respectively, see Sketch 1.1

For tailplanes mounted on the body or for cases where there is no tailplane

$$\overline{z_F^*} = z_{crF} + 0.6h_F \tag{3.4}$$

and

$$\overline{l_F^*} = m_F + 0.6h_F\tan\Lambda_{¼F}\,. \tag{3.5}$$

For tailplanes mounted on the fin

$$\overline{z_F^*} = z_{crF} + \{0.5h_F + 0.2|z_T - 0.5h_F|\} \tag{3.6}$$

and

$$\overline{l_F^*} = m_F + \{0.5h_F + 0.2|z_T - 0.5h_F|\}\tan\Lambda_{¼F}\,. \tag{3.7}$$

The factors K_1, K_2 and K_3 (see Section 3.2) are given in Figures 1a to 1c. The factor K_1 in Figure 1a is a function of fin aspect ratio A_F and fin sweep $\Lambda_{¼F}$ and represents the contribution of the vertical fin to the fin damping. The factors K_2 and K_3 allow for interference effects of the tailplane on the fin.

For fin-mounted tailplanes K_2 is a function of the ratio of tailplane span to fin height b_T/h_F and fin sweep $\Lambda_{¼F}$, and is given in Figure 1b. The factor K_3 is a function of the ratio of tailplane height to fin height z_T/h_F, and is given in Figure 1c. The product K_2K_3 is added to K_1 to allow for tailplane interference, which in the case of fin-mounted tailplanes increases the magnitude of the fin damping.

For body-mounted tailplanes K_2 has a constant value of –0.05. Tailplane height has no effect in this case so K_3 is equal to 1 in Equation (3.1) and K_2 is simply added to K_1. In this case the tailplane interference acts to reduce the magnitude of the fin damping.

Equations (3.4) to (3.7) that define the centre of pressure position of the fin in terms of the fin height h_F, the fin sweep $\Lambda_{¼F}$ and the tailplane height z_T (see Sketch 1.1) are discussed in Section 3.2.

The geometric properties of the fin are defined in the same way as they are in Item No. 82010 (Reference 26) for calculating the fin static lateral stability derivatives due to sideslip. Thus the fin tip chord c_{tF} is the chordwise distance between the leading and trailing edges of the fin at the maximum fin height. The fin root chord c_{rF} is the chordwise distance between the leading and trailing edges of the fin at the height where the fin quarter-chord sweep line intersects the top of the body (see Sketch 1.1), with any dorsal fin extension to the fin leading-edge being ignored. The fin height h_F is the perpendicular distance between the fin root and tip chords. The fin area S_F is the area enclosed by the leading and trailing edges of the fin (again ignoring any dorsal extension) and the fin tip and root chords, so that

$$S_F = h_F(c_{rF} + c_{tF})/2\,. \tag{3.8}$$

The effective aspect ratio of the fin is obtained for the straight-tapered wing formed by reflecting the fin about its root chord, so that

$$A_F = 2h_F^2\ /S_F\,. \tag{3.9}$$

The wing sidewash parameter $\partial\bar{\sigma}_W/\partial(pb/V)$ in Equation (3.1) allows for interference between the wing and fin (which has a large effect on the roll rate derivatives as illustrated in Sketch 2.1). The wing sidewash is discussed in Section 3.3 and a constant value of 0.18 is substituted for $\partial\bar{\sigma}_W/\partial(pb/V)$ in Equation (3.1).

The sidewash parameter $\partial\bar{\sigma}_\alpha/\partial(pb/V)$ in Equation (3.1) is given in Figure 2 as a function of $[\overline{z_F^*} - (\overline{z_F^*}\cos\alpha - \overline{l_F^*}\sin\alpha)]/b$. It has been derived empirically from comparisons with a large number of experimental data and it allows for changes in the sidewash that occur at the fin as α increases, and for changes in the fin effectiveness that may be expected to occur as the roll rate axis approaches and eventually intersects the fin as α increases. It is discussed further in Section 3.4.

3.1.1 Mach number effects

Equations (3.1) to (3.3) have been derived from low speed data and contain no allowance for compressibility effects. Examination of the experimental variations with Mach number that are given in Derivations 8, 12 to 15 and 18 show that up to about Mach 0.8 the effects of compressibility are usually small, causing changes of about ± 0.01 in $(Y_p)_F$, ± 0.004 in $(N_p)_F$ and ± 0.003 in $(L_p)_F$. However, these changes do not occur in a predictable manner and it is therefore recommended that the predictions of Equations (3.1) to (3.3) be used at all subsonic Mach numbers for which the flow over the aircraft is wholly subsonic and fully attached. Above Mach 0.8, and sometimes at lower Mach numbers depending on the aircraft configuration, the appearance of shock waves or of flow separation can cause large changes in the roll rate derivatives, as shown in Derivation 15 for example. Naturally, in such cases large departures from the predicted values are to be expected.

3.1.2 Tailplane contribution

If the tail assembly includes a tailplane then this also provides a contribution, $(L_p)_T$, to L_p although this is usually small. In the absence of the wing and body the theoretical predictions of Derivations 10, 16 and 20 show that isolated wing data provide a good estimate of the tailplane contribution, any interference from the fin being negligible, see Section 3.2.1. When the wing and body are present Derivation 6 suggests that $(L_p)_T$ can be estimated by calculating L_p for the tailplane as an isolated wing and factoring the result by $0.5\ S_T b_T^2/S_W b^2$, where the factor 0.5 is included to account for the rotation of the flow produced by the wing. (The other factors convert to the correct reference area and span.) Item No. Aero A.06.01.01 (Reference 23) provides suitable data on L_p for isolated wings. This estimate of the tailplane effect can only be regarded as approximate but it has been adopted in several references, such as Reference 24. Since $(L_p)_T$ is only a small part of the total value of L_p for an aircraft any errors involved in estimating its

magnitude will not be important. However, its magnitude is significant when compared to $(L_p)_F$ and it should be added to the prediction of Equation (3.3) when estimating the total effect of a tail assembly.

3.2 Derivation of Factors K_1, K_2 and K_3

The factors K_1, K_2 and K_3 have been developed by interpolating between the theoretical results reported in Derivations 10, 16 and 20 (which are restricted in scope, see Section 3.2.1) and by applying some empirical corrections after comparisons with experimental data. In Derivations 10, 16 and 20 the theoretical spanwise loadings arising on an isolated fin and horizontal tailplane assembly (no body, no wing) rolling about the fin root chord are calculated by using a finite-step technique in which the vertical and horizontal surfaces are represented by a number of horseshoe vortices, and the roll rate derivatives are found by integration of the loadings.

Sketch 3.1 shows typical predicted loadings for a fin with a tailplane situated either at the fin root or at the top of the fin. The loading across the tailplane is antisymmetric and contributes to L_p, but not to Y_p or N_p.

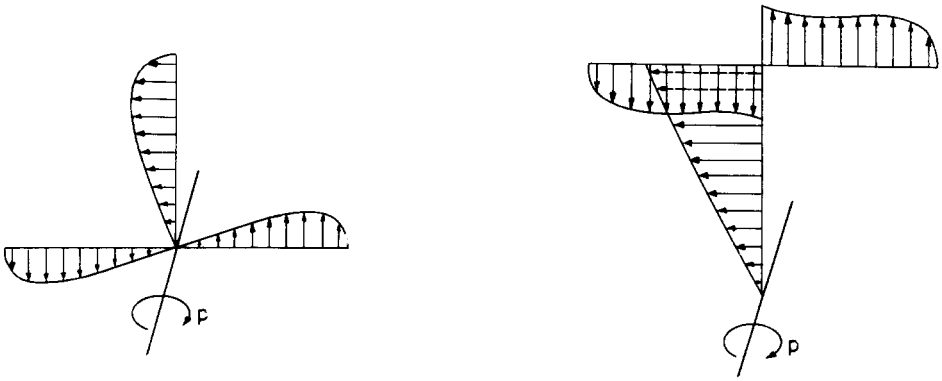

Sketch 3.1 Illustration of loading distributions on isolated fin and tailplane. Rolling about fin root.

The theoretical predictions have been analysed by dividing the total damping into a fin component and a tailplane-fin interference component. The fin component is mainly a function of fin aspect ratio and varies little with fin sweep angle. The tailplane-fin interference component depends on the ratio of the tailplane span to the fin height. For tailplanes mounted high on the fin it is also very dependent on fin sweep. For unswept fins, tailplanes mounted high on the fin cause a large increase in the fin damping which increases with tailplane span, but this effect largely disappears for fins swept 45°. For tailplanes mounted at the fin root, a (smaller) reduction in the fin damping is predicted, which is again less significant for swept fins than for unswept fins. Tailplanes mounted at the fin mid-point have no effect. Comparisons with experimental data confirm that configurations with tailplanes mounted high on the fin have high values of roll damping consistent with the theoretical values, but for tailplanes mounted on the body better agreement is achieved if the reduction in damping due to the tailplane-fin interference is assumed to be less than that predicted and independent of the fin-tailplane geometry.

Because the range of data in Derivations 10, 16 and 20 is limited (see Section 3.2.2) interpolations in fin sweep angle between 0 and 45° and in tailplane height between fin root, mid fin and fin tip have been necessary. Figures 1a to 1c shows the values of K_1, K_2 and K_3 that have been developed for general use. The variation with fin sweep angle has been taken to be similar to that for the isolated wing data on L_p given in Item No. Aero A.06.01.01 (Reference 23). For fin-mounted tailplanes the variation of K_3 with tailplane height has been chosen to give a reasonable increase in tailplane-fin interference as the tailplane height on the fin increases, with the effect disappearing for tailplanes mounted below the fin mid-point.

The factors K_1, K_2 and K_3 in Figures 1a to 1c are based on fin area and height as reference dimensions. Therefore, converting to the wing area and span the damping derivative Y_p at zero angle of attack, relative to the fin root chord as roll axis, is given by

$$(Y_p)_F = -(K_1 + K_2K_3)\frac{S_F h_F}{S_W b}. \tag{3.10}$$

This is converted to the proper rolling moment axis at a distance z_{crF} below the fin root chord by multiplying by $\overline{z_F^*}/(\overline{z_F^*} - z_{crF})$, so that

$$(Y_p)_F = -(K_1 + K_2K_3)\frac{S_F h_F}{S_W b}\frac{\overline{z_F^*}}{(\overline{z_F^*} - z_{crF})}, \tag{3.11}$$

with $$(N_p)_F = -(Y_p)_F \overline{l_F^*}/b. \tag{3.12}$$

and $$(L_p)_F = (Y_p)_F \overline{z_F^*}/b. \tag{3.13}$$

These equations have been found to give a good prediction of the fin effect on the roll-rate derivatives in the case of models tested without wings and at zero angle of attack, the situation to which the basic theoretical data in Derivations 10, 16 and 20 apply most closely. The modifications that are made to allow for the presence of the wing and for variations with angle of attack are discussed in Sections 3.3 and 3.4.

The vertical location of the centre of pressure of the roll damping force on the fin has also been estimated from the results presented in Derivations 10, 16 and 20, by considering values of L_p/Y_p. These indicate that for tailplanes mounted at the root or at the top of the fin the centre of pressure position is at about 60 per cent of the fin height above the fin root chord. As the ratio of tailplane span to fin height increases there is a predicted movement of the centre of pressure towards the fin tip for tailplanes at the fin root and towards the fin root for tailplanes mounted at the top of the fin. However, a constant value of $0.6h_F$ has been assumed for these two cases and this is also the value predicted for the fin alone. For tailplanes mounted at the fin mid-point the centre of pressure position is also at the fin mid-point and a linear variation with tailplane height (z_T/h_F) has been assumed to allow for variations between this and the value of $0.6h_F$ for tailplanes at either extremity of the fin. The longitudinal position of the centre of gravity is determined by assuming it lies on the fin quarter-chord sweep line. These results are summarised in Equations (3.4) to (3.7), where the distances m_F and z_{crF} have been added to the longitudinal and vertical positions to correct the moment arms to the aircraft centre of gravity position.

3.2.1 Fin-tailplane interference

The values of $(L_p)_T$ predicted by the methods in Derivations 10, 16 and 20, which arise from the antisymmetric loadings illustrated in Sketch 3.1, are very close to those obtained by using the isolated wing data in Item No. Aero A.06.01.01 (Reference 23), the experimental magnitudes being typically 10 per cent higher for tailplanes mounted at the top of the fin and less than 5 per cent higher for tailplanes at the fin root. This shows that to a good approximation the interference of the fin on the tailplane can be neglected, and in the case where no wing is present the tailplane contribution can be estimated as for a wing in isolation, but as stated in Section 3.1.2 the presence of the wing reduces the tailplane contribution by about half.

3.2.2 Note on data in Derivations 10, 16 and 20

The data in Derivations 10 and 16 are restricted in scope. Derivation 10 covers unswept and 45° sweptback fin and tailplane assemblies for which the taper ratio of both surfaces is always equal to 0.5, with the fin aspect ratio taking values of 1, 2 and 3[†] and the ratio of tailplane to fin aspect ratio being 1, 2 or 3 in each case. The tailplane is positioned in turn at the foot, at the mid-point and at the top of the fin. In Derivation 10 the root chord of the fin and the centre-line chord of the tailplane are equal, with the tailplane centre-line quarter-chord point being located at the fin local quarter-chord point; thus for the case of tailplanes mounted at the mid-point or top of the fin the tailplane extends forward of the fin leading-edge. Derivation 16 considers only unswept fins and tailplanes of taper ratio 0.5, with the fin aspect ratio equal to 1, and with the ratio of the tailplane span to the fin height taking values of 4/3, 8/3 and 4. Tailplane positions at the foot, the mid-point and the top of the fin are again considered, and in this case variations of the ratio of the tailplane centre-line chord to the fin root chord from 0 to 1 are also treated for each arrangement, with the centre-line quarter-chord point of the tailplane always coinciding with the local quarter-chord point of the fin.

Derivation 20 recommends that the data in Derivation 16 can be used to define a correction factor allowing for variations of the ratio of tailplane centre-line chord to fin root chord, c_{0T}/c_{rF}, for fin aspect ratios of unity, and that in the absence of other information this correction factor can be applied at all fin aspect ratios. This approach has been used to convert the data in Derivations 10 and 16 to the more practical situation where the tailplane centre-line chord is equal to the local fin chord prior to the analysis that has been carried out for this Item.

3.3 Sidewash Due to Wing

In rolling flight an antisymmetric spanwise loading is generated over a wing, and the trailing vortices associated with this loading give rise to a sideslip velocity distribution over the fin which opposes the sideslip velocity due to the rolling of the fin itself. This is discussed in detail in Derivation 5 and is illustrated in Sketch 3.2. If the mean effective sidewash angle at the centre of pressure of the rolling fin is $\bar{\sigma}_W$, then at zero angle of attack the effect on the predicted roll rate derivative Y_p is to reduce the moment arm in the numerator of Equation (3.11) from $\bar{z}_F^*$ to $(\bar{z}_F^*/b - \partial\bar{\sigma}_W/\partial(pb/V))b$.

Comparisons with experimental values of $(Y_p)_F$ and $(N_p)_F$ obtained at $\alpha = 0$ and the predictions of Equations (3.11) and (3.12) modified in this manner indicate that good overall agreement between prediction and experiment is obtained if a constant value of 0.18 is taken for $\partial\bar{\sigma}_W/\partial(pb/V)$. Attempts to allow for variations of this parameter with aircraft geometry, using the method of Derivation 5 as basis, have been made but do not lead to any improvement in prediction.

Derivations 3 and 5 show from comparisons with experimental data that an adequate representation of the wing effect on the fin characteristics is obtained by assuming that the wing sidewash term does not vary with α, at least for an angle of attack ranging from 0 to 15°. The method in this Item follows this approach and $\partial\bar{\sigma}_W/\partial(pb/V)$ is therefore assumed to be invariant with both aircraft geometry and angle of attack.

[†] The aspect ratio of the isolated fin is half of that which would result from Equation (3.9) and these therefore correspond to $A_F = 2, 4$ and 6.

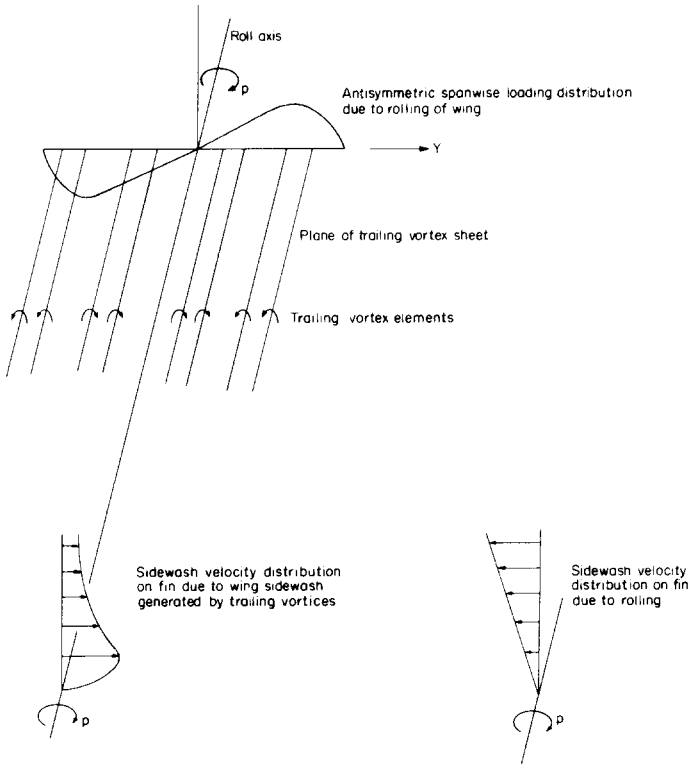

Sketch 3.2 Illustration of sidewash velocity distributions on fin for zero angle of attack and unswept wing

3.4 Variations with Angle of Attack

Although the effect of the wing sidewash at the fin is assumed to be independent of the angle of attack, Derivation 3 shows from comparisons with experimental data, for both wing-on and wing-off models, that at non-zero angles of attack a significantly improved representation of the flow at the fin is obtained when allowance is made for the presence of a body sidewash term which increases with α. It is also to be expected that as α increases and the fin approaches and intersects the roll axis then the contributions of the fin to the damping derivatives will alter when parts of the fin lie to either side of the roll axis.

A single parameter, $\partial\bar{\sigma}_\alpha/\partial(pb/V)$, has been introduced to incorporate both of these angle of attack effects, so that at any angle of attack α the moment arm in the numerator of Equation (3.11) changes from $\bar{z}_F^*$ to

$$[(\bar{z}_F^* \cos\alpha - \bar{l}_F^* \sin\alpha)/b - \partial\bar{\sigma}_W/\partial(pb/V) - \partial\bar{\sigma}_\alpha/\partial(pb/V)]b$$

where the first term is simply a geometric effect. Equation (3.11) is then converted into Equation (3.1) and Equations (3.12) and (3.13) become Equations (3.2) and (3.3) after the geometric substitutions of $(\bar{l}_F^* \cos\alpha + \bar{z}_F^* \sin\alpha)$ for $\bar{l}_F^*$ and $(\bar{z}_F^* \cos\alpha - \bar{l}_F^* \sin\alpha)$ for $\bar{z}_F^*$.

Comparisons of the predictions of Equations (3.1) to (3.3) for a large number of experimental data have enabled a simple estimate of $\partial\bar{\sigma}_\alpha/\partial(pb/V)$ to be made which varies only with $[\bar{z}_F^* - (\bar{z}_F^* \cos\alpha - \bar{l}_F^* \sin\alpha)]/b$, as shown in Figure 2, (a variation of body sidewash with this parameter is suggested in Derivation 3). Despite the crudeness of this treatment of a complex interaction good agreement with the experimental variation of the roll rate stability derivatives with α is obtained for many different configurations for angles of attack up to about 15° or 20°, or until the appearance of flow separation effects begins to make accurate predictions impracticable.

4. ACCURACY AND APPLICABILITY

4.1 Accuracy

The overall accuracy of prediction in magnitude for the roll rate derivatives is summarised in Sketch 4.1. Generally, $(Y_p)_F$ is predicted to within ±0.03 and $(N_p)_F$, the most important derivative, to within ±0.015. The total contribution of the tail assembly, $(L_p)_F + (L_p)_T$, is generally predicted to within ±0.01.

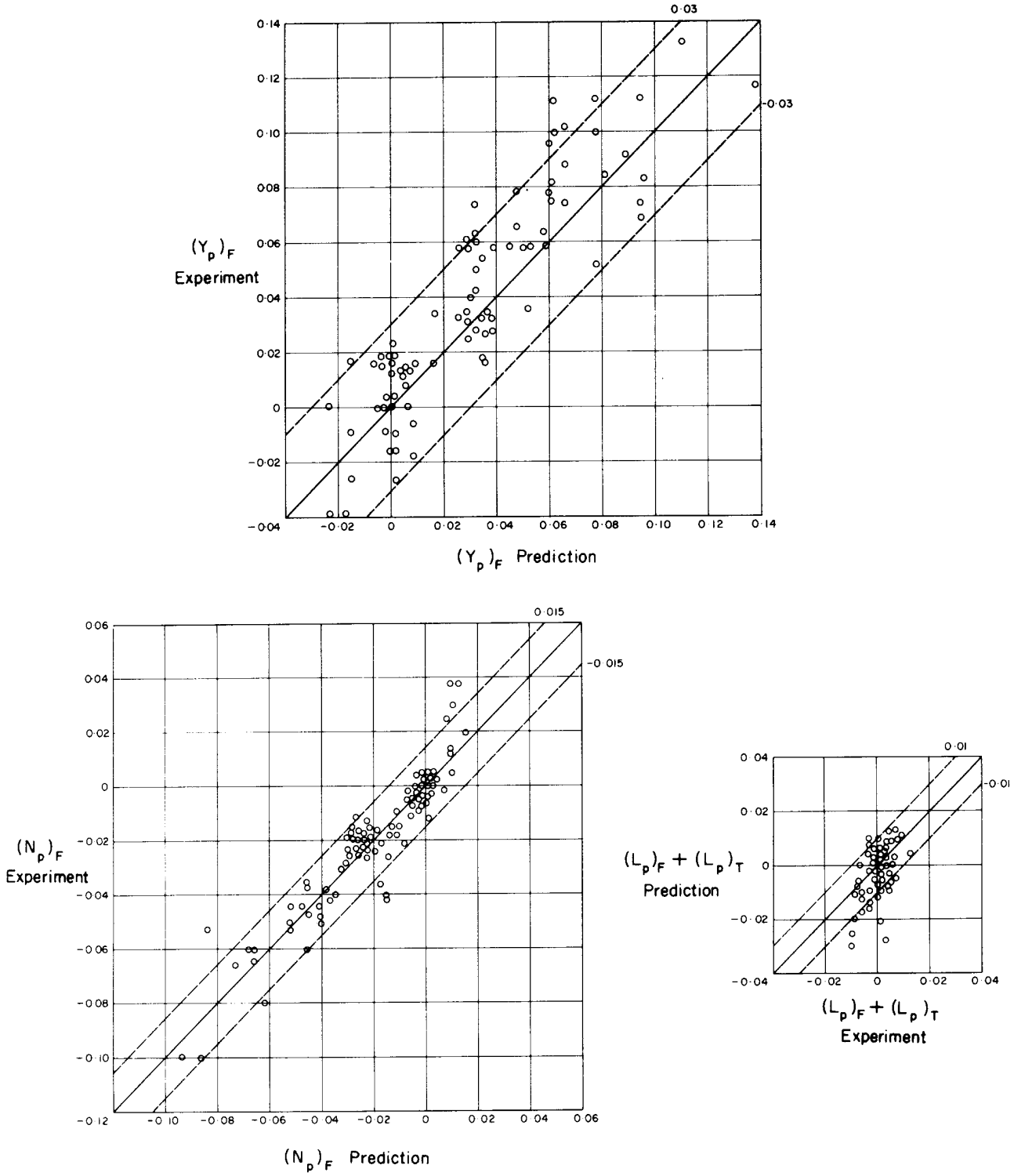

Sketch 4.1 Comparisons of experimental and predicted derivatives

The variation of $(Y_p)_F$ and $(N_p)_F$ with angle of attack is usually predicted well for angles of attack up to about 15° or 20° or until flow separation occurs. In most cases the level of accuracy achieved at $\alpha = 0$ is maintained as α increases, although there is a slight worsening of prediction towards the higher angles of attack. The variation of the tail assembly contribution to L_p is not predicted quite so well, but this is thought to be partly due to the difficulty of identifying the small contribution of the tail assembly from fin-on and fin-off experimental tests. Since the tail assembly contributes only a small part of the total aircraft value of L_p, any shortcomings in the prediction are not significant.

4.2 Applicability

Comparisons with the experimental data in Derivations 1 to 4, 6 to 9, 11 to 15, 17 to 19, 21 and 22 have shown that the method provides satisfactory predictions of roll rate derivatives for a wide variety of wing-body-tail geometries, for cases where no flaps or slats are deployed. Table 4.1 summarises the range of the more important parameters that have been covered. The method is applicable for subsonic flight speeds up to $M = 0.8$ provided the flow over the aircraft is wholly subsonic and fully attached, Separation of the flow over the wing or tail will lead to poor agreement between the predicted and experimental contributions of the tail assembly.

TABLE 4.1 Range of Geometric Parameters

A_W	1.5 to 7	A_F	1.6 to 4.3	A_T	1.8 to 4
$\Lambda_{¼W}$	0 to 70°	$\Lambda_{¼F}$	0 to 50°	$\Lambda_{¼T}$	0 to 45°
λ	0 to 1	λ_F	0 to 1	λ_T	0 to 1
$\overline{z_F^*}/b$	0.13 to 0.25	b_T/h_F	2 to 3		
$\overline{l_F^*}/b$	0.22 to 0.75	z_T/h_F	0.25 to 1		

5. DERIVATION AND REFERENCES

5.1 Derivation

The Derivation lists selected sources that have assisted in the preparation of this Item.

1. BIRD, J.D. LICHTENSTEIN, J.H. JAQUET, B.M. — Investigation of the influence of fuselage and tail surfaces on low-speed static stability and rolling characteristics of a swept-wing model. NACA tech. Note 2741, 1947.
2. LETKO, W. RILEY, D.R. — Effect of an unswept wing on the contribution of unswept-tail configurations to the low-speed static- and rolling-stability derivatives of a midwing airplane model. NACA tech. Note 2175, 1950.
3. WOLHART, W.D. — Influence of wing and fuselage on the vertical-tail contribution to the low-speed rolling derivatives of midwing airplane models with 45° sweptback surfaces. NACA tech. Note 2587, 1951.
4. FISHER, L.R. MICHAEL, W.H. — An investigation of the effect of vertical-fin location and area on low-speed lateral stability derivatives of a semitailless airplane model. NACA RM L51A10 (TIL 2655), 1951.
5. MICHAEL, W.H. — Analysis of the effects of wing interference on the tail contributions to the rolling derivatives. NACA Rep. 1086, 1952.

6. CAMPBELL, J.P. McKINNEY, M.O. — Summary of methods for calculating dynamic lateral stability and response and for estimating lateral stability derivatives. NACA Rep. 1098, 1952.

7. GOODMAN, A. THOMAS, D.F. — Effects of wing position and fuselage size on the low-speed static and rolling stability characteristics of a delta-wing model. NACA tech. Note 3063, 1953.

8. KUHN, R.E. WIGGINS, J.W. — Wind-tunnel investigation to determine the aerodynamic characteristics in steady roll of a model at high subsonic speeds. NACA RM L52K24 (TIL 3581), 1953.

9. WILLIAMS, J.L. — Measured and estimated lateral static and rotary derivatives of a 1/12-scale model of a high-speed fighter with unswept wings. NACA RM L53K09 (TIL 5187), 1954.

10. QUEIJO, M.J. RILEY, D.R. — Calculated subsonic span loads and resulting stability derivatives of unswept and 45° sweptback tail surfaces in sideslip and steady roll. NACA tech. Note 3245, 1954.

11. FISHER, L.R. LICHTENSTEIN, J.H. WILLIAMS, K.D. — A preliminary investigation of the effects of frequency and amplitude on the rolling derivatives of an unswept-wing model oscillating in roll. NACA tech. Note 3554, 1955.

12. SLEEMAN, W.C. WIGGINS, J.W. — Experimental investigation at high subsonic speeds of the rolling stability derivatives of a complete model with an aspect-ratio-2.52 wing having an unswept 72-percent-chord line and a high horizontal tail. NACA RM L54I20 (TIL 6633), 1955.

13. BEAM, B.H. REED, V.D. — Wind-tunnel measurements at subsonic speeds of the static and dynamic-rotary stability derivatives of a triangular-wing airplane model having a triangular vertical tail. NACA RM A55A28, 1955.

14. SLEEMAN, W.C. FEW, A.G. — Experimental investigation at high subsonic speed of the rolling stability derivatives of a complete model having a clipped-delta wing and a high horizontal tail. NACA RM L55K11 (TIL 4978), 1955.

15. BUELL, D.A. VERLIN, D.R. LOPEZ, A.E. — The static and dynamic-rotary stability derivatives at subsonic speeds of an airplane model with an unswept wing and a high horizontal tail. NACA RM A56I04 (TIL 6655), 1956.

16. BOOTH, K.W. — Effect of horizontal-tail chord on the calculated subsonic span loads and stability derivatives of isolated unswept tail assemblies in sideslip and steady roll. NASA Memo. 4-1-59L (TIL 6304), 1959.

17. FISHER, L.R. — Experimental determination of the effects of frequency and amplitude of oscillation on the roll-stability derivatives for a 60° delta-wing airplane model. NASA tech. Note D-232, 1960.

18. HENDERSON, W.P. PHILLIPS, W.P. GAINER, T.G. — Rolling stability derivatives of a variable-sweep tactical fighter model at subsonic and transonic speeds. NASA tech. Note D-3845, 1967.

19. GRAFTON, S.B. CHAMBERS, J.R. COE, P.L. — Wind-tunnel free-flight investigation of a model of a spin-resistant fighter configuration. NASA tech. Note D-7716, 1974.

20. RILEY, D.R. — Determination of stability derivatives of isolated rigid tail assemblies in sideslip and steady roll. AIAA Paper No. 74-1038, 1974.

21. O'LEARY, C.O. — Wind-tunnel measurements of lateral aerodynamic derivatives using a new oscillatory rig, with results and comparisons for the Gnat aircraft. ARC R&M 3847, 1977.

22. RAE — Unpublished wind tunnel results.

5.2 References

The References list selected sources of information supplementary to that given in this Item.

23. ESDU — Stability derivative L_p, rolling moment due to rolling for swept and tapered wings. Item No. Aero. A.06.01.01. Engineering Sciences Data Unit, London, March 1955.

24. WOLOWICZ, C.H. YANCEY, R.B. — Lateral-directional aerodynamic characteristics of light, twin-engine, propeller-driven airplanes. NASA tech. Note D-6946, 1972.

25. ESDU — Contribution of wing planform to derivatives of yawing moment and sideforce due to roll rate at subsonic speeds, $(N_p)_w$ and $(Y_p)_w$. Item No.81014, Engineering Sciences Data Unit, London, June 1981.

26. ESDU — Contribution of fin to sideforce, yawing moment and rolling moment derivatives due to sideslip, $(Y_v)_F$, $(N_v)_F$, $(L_v)_F$, in the presence of body, wing and tailplane. Item No.82010, Engineering Sciences Data Unit, London, April 1982.

6. EXAMPLE

Calculate the contribution of the tail assembly to the roll rate derivatives Y_p, N_p and L_p for the model configuration in Sketch 6.1 for the three wing positions shown, at angles of attack up to 20° . Compare the results with the experimental data for this model that are given in Derivation 18. The wing reference area S_W is 0.101 m^2 and the reference span b is 0.873 m.

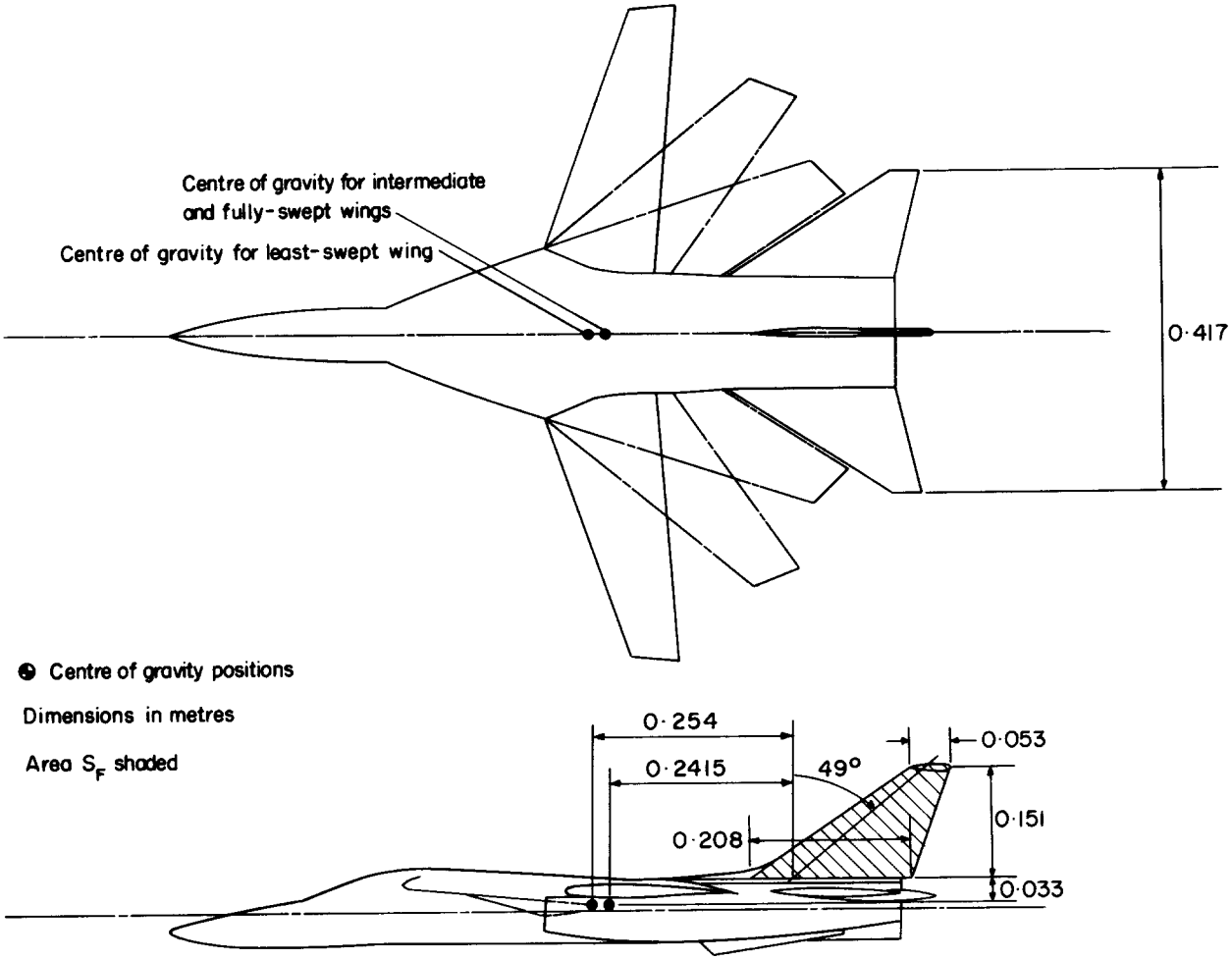

Sketch 6.1

From the dimensions given in Sketch 6.1, the fin root chord, tip chord, height and sweep are respectively,

$$c_{rF} = 0.208 \text{ m}, \; c_{tF} = 0.053 \text{ m}, \; h_F = 0.151 \text{ m}, \text{ and } \Lambda_{¼F} = 49° .$$

The fin area is obtained from Equation (3.8)

$$S_F = h_F(c_{rF} + c_{tF})/2$$

$$= 0.151(0.208 + 0.053)/2 = 0.0197 \text{ m}^2 .$$

The fin aspect ratio is obtained from Equation (3.9)

$$A_F = 2h_F^2 / S_F$$

$$= 2 \times 0.151^2 / 0.0197 = 2.31.$$

Therefore from Figure 1a, $K_1 = 0.81$.

As the tailplane is body-mounted, $K_2 = -0.05$ and $K_3 = 1$.

(Had the tailplane been fin-mounted, K_2 would have been found from Figure 1b as a function of $\Lambda_{¼F}$ and b_T / h_F, and K_3 would have been found from Figure 1c as a function of z_T / h_F.)

The centre of pressure position is calculated from Equations (3.4) and (3.5). For the least-swept wing $m_F = 0.254$ m and $z_{crF} = 0.033$ m, so

$$\overline{z_F^*} = z_{crF} + 0.6h_F$$

$$= 0.033 + 0.6 \times 0.151 = 0.124 \text{ m}$$

and

$$\overline{l_F^*} = m_F + 0.6h_F \tan\Lambda_{¼F}$$

$$= 0.254 + 0.6 \times 0.151 \times \tan 49 = 0.358 \text{ m}.$$

The wing sidewash parameter $\partial\bar{\sigma}_W/\partial(pb/V)$ is, as discussed in Section 3.3, taken to be constant at 0.18.

The parameter $\partial\bar{\sigma}_\alpha/\partial(pb/V)$ which allows for changes in sidewash due to changes of angle of attack is obtained from Figure 2 as a function of

$$[\overline{z_F^*} - (\overline{z_F^*} \cos\alpha - \overline{l_F^*} \sin\alpha)]/b.$$

With $\overline{z_F^*} = 0.124$ m, $\overline{l_F^*} = 0.358$ m and $b = 0.873$ m, Table 6.1 sets out the results obtained for $0 \le \alpha \le 20°$.

TABLE 6.1

α (deg)	0	4	8	12	16	20
$[\overline{z_F^*} - \overline{z_F^*}(\cos\alpha - \overline{l_F^*}\sin\alpha)]/b$	0	0.029	0.058	0.088	0.119	0.149
$\partial\bar{\sigma}_\alpha/\partial(pb/V)$	0	0.042	0.087	0.136	0.188	0.244

The derivatives $(Y_p)_F$, $(N_p)_F$ and $(L_p)_F$ are obtained from Equations (3.1) to (3.3),

$$(Y_p)_F = -(K_1 + K_2K_3)\frac{S_F h_F}{S_W b}\left\{\frac{(\overline{z_F^*}\cos\alpha - \overline{l_F^*}\sin\alpha)/b - \partial\bar{\sigma}_W/\partial(pb/V) - \partial\bar{\sigma}_\alpha/\partial(pb/V)}{(\overline{z_F^*} - z_{crF})/b}\right\},$$

$$(N_p)_F = -(Y_p)_F(\overline{l_F^*}\cos\alpha + \overline{z_F^*}\sin\alpha)/b,$$

and $(L_p)_F = (Y_p)_F(\overline{z}_F^* \cos\alpha - \overline{l}_F^* \sin\alpha)/b$.

The results of this are set out in Table 6.2.

TABLE 6.2

α (deg)	0	4	8	12	16	20
$\dfrac{\overline{z}_F^* \cos\alpha - \overline{l}_F^* \sin\alpha}{b}$	0.142	0.133	0.084	0.054	0.023	–0.007
$\dfrac{\overline{l}_F^* \cos\alpha + \overline{z}_F^* \sin\alpha}{b}$	0.410	0.419	0.426	0.431	0.433	0.434
$\dfrac{\partial\bar{\sigma}_W}{\partial(pb/V)}$	0.18	0.18	0.18	0.18	0.18	0.18
$\dfrac{\partial\bar{\sigma}_\alpha}{\partial(pb/V)}$	0	0.042	0.087	0.136	0.188	0.244
$(Y_p)_F$	0.009	0.027	0.045	0.065	0.085	0.106
$(N_p)_F$	–0.004	–0.011	–0.019	–0.028	–0.037	–0.046
$(L_p)_F$	0.001	0.003	0.004	0.003	0.002	–0.001

The tailplane contribution to L_p, $(L_p)_T$, is estimated as discussed in Section 3.1.2 by using Item No. Aero A.06.01.01 (Reference 23) to estimate a value of L_p as though for an isolated wing and reducing that value by half to allow for the rotation of the flow produced by the wing. The tailplane in Sketch 6.1 has an aspect ratio $A_T = 2.32$, a quarter-chord sweep $\Lambda_{¼T} = 52°$ and a taper ratio $\lambda_T = 0.12$. Assuming an incompressible section lift-curve slope of 2π for the tailplane, Item No. Aero A.06.01.01 gives an isolated wing value of $L_p = -0.09$ based on the tailplane area $S_T = 0.075$ m^2 and span $b_T = 0.417$ m.

This is converted to a contribution to the aircraft L_p through the equation

$$\begin{aligned}(L_p)_T &= -0.09 \times 0.5 \times S_T b_T^2 / S_W b^2 \\ &= -0.09 \times 0.5 \times 0.075 \times 0.417^2 / 0.101 \times 0.873^2 \\ &= -0.008.\end{aligned}$$

This is added to $(L_p)_F$ to estimate the total contribution of the tail assembly to L_p.

Sketch 6.2a shows the contributions $(Y_p)_F$, $(N_p)_F$ and $(L_p)_F + (L_p)_T$ plotted against α for the configuration with the least-swept wing. Experimental results from Derivation 18 are shown for comparison.

Sketches 6.2b and 6.2c show similar comparisons for the intermediate and fully-swept wings. In these two cases the derivatives have been predicted using the true wing span and area and then converted to values based on $S_W = 0.101$ m^2 and $b = 0.873$ m.

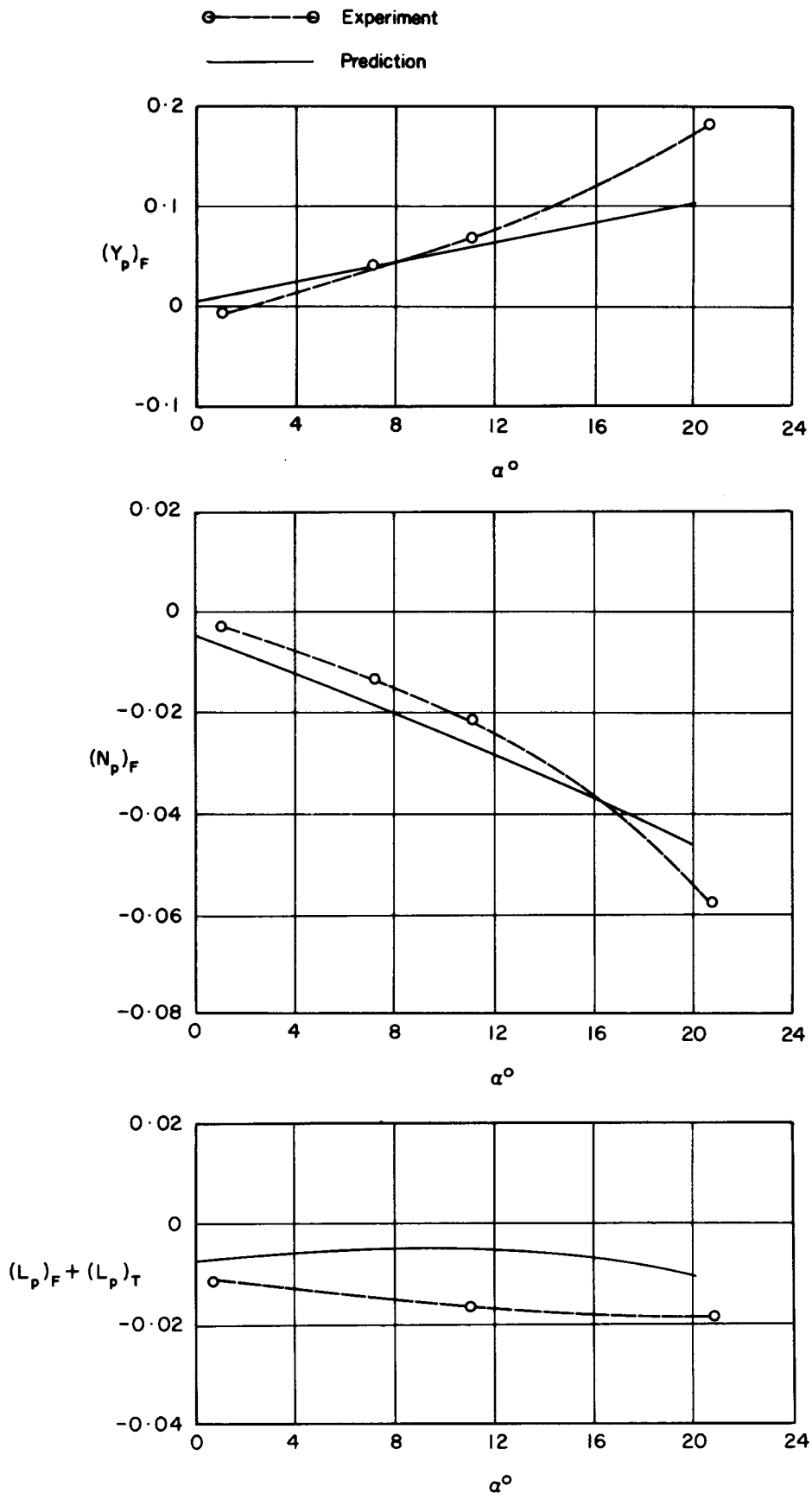

Sketch 6.2a Least-swept wing

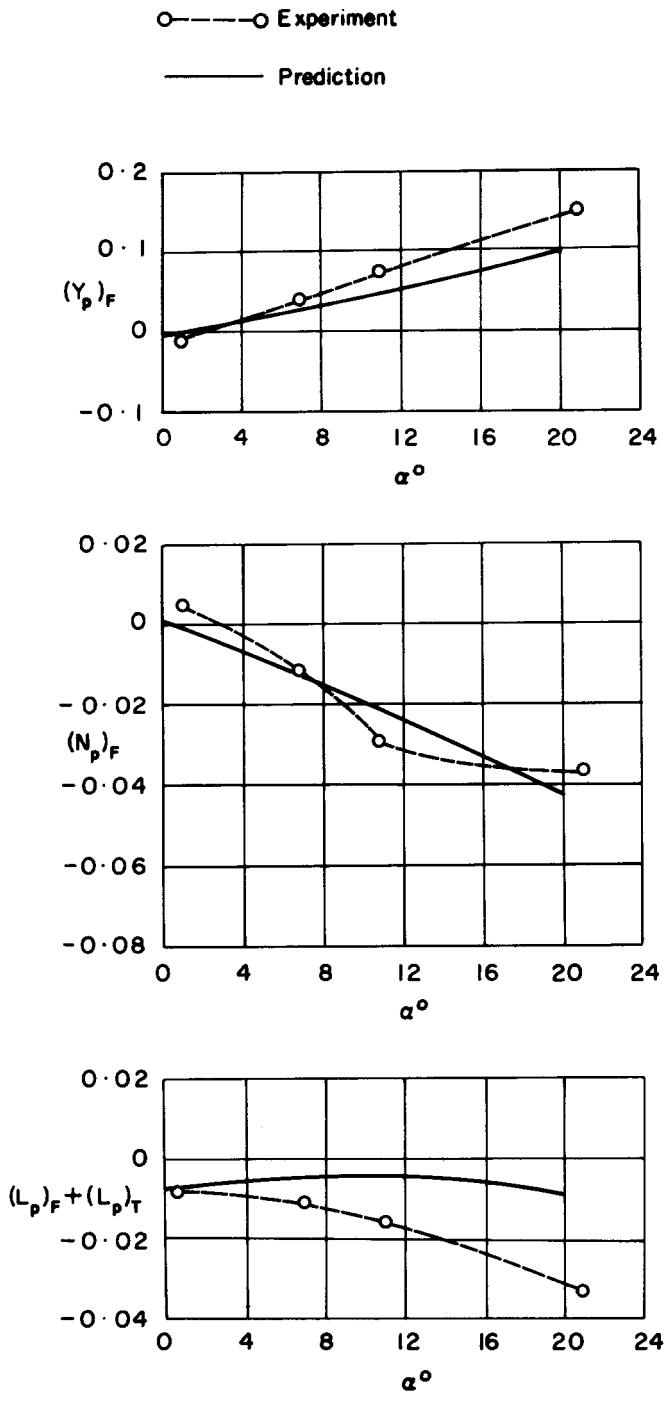

Sketch 6.2b Intermediate wing

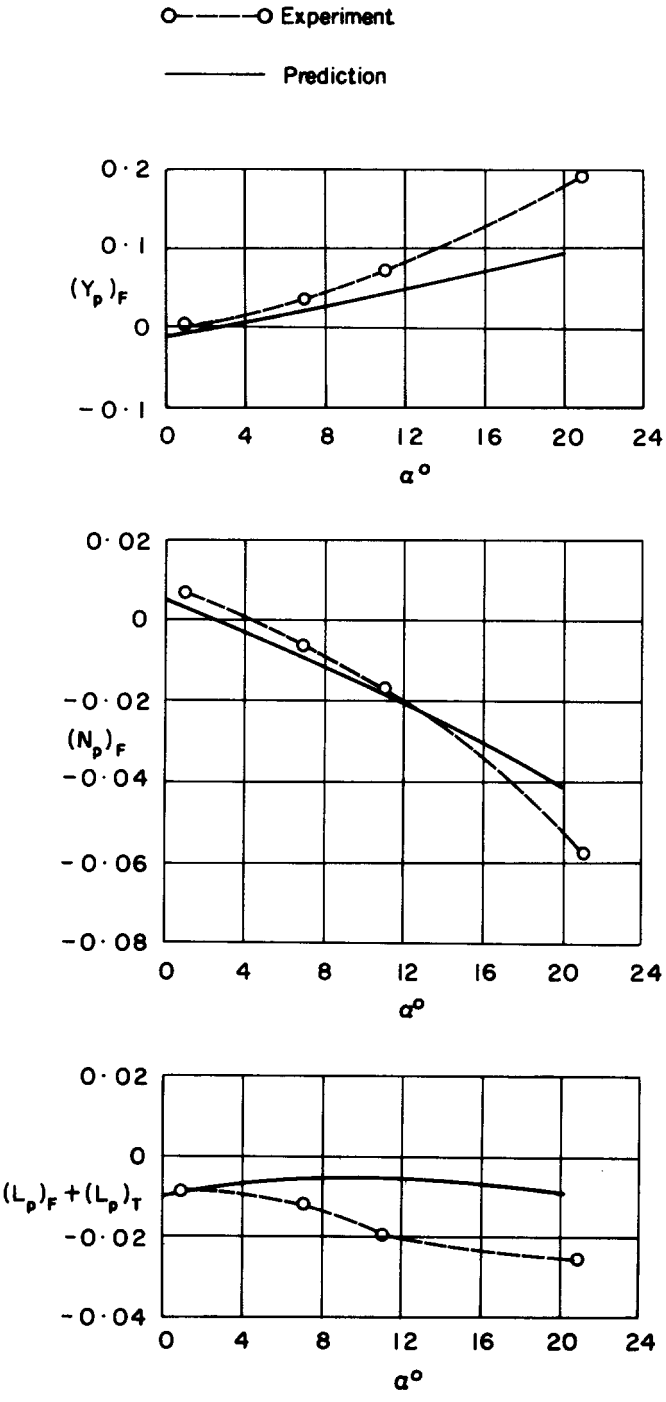

Sketch 6.2c Fully-swept wing

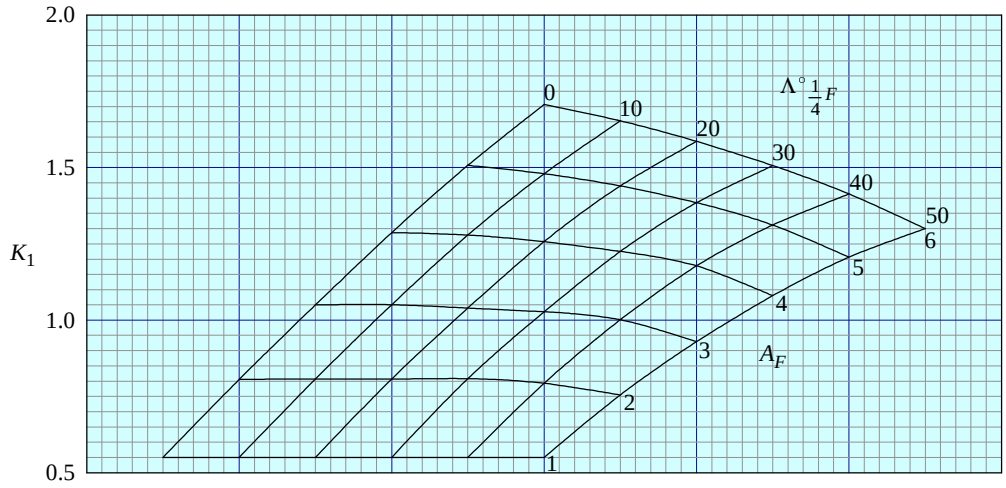

FIGURE 1a FIN ROLL-DAMPING PARAMETER K_1

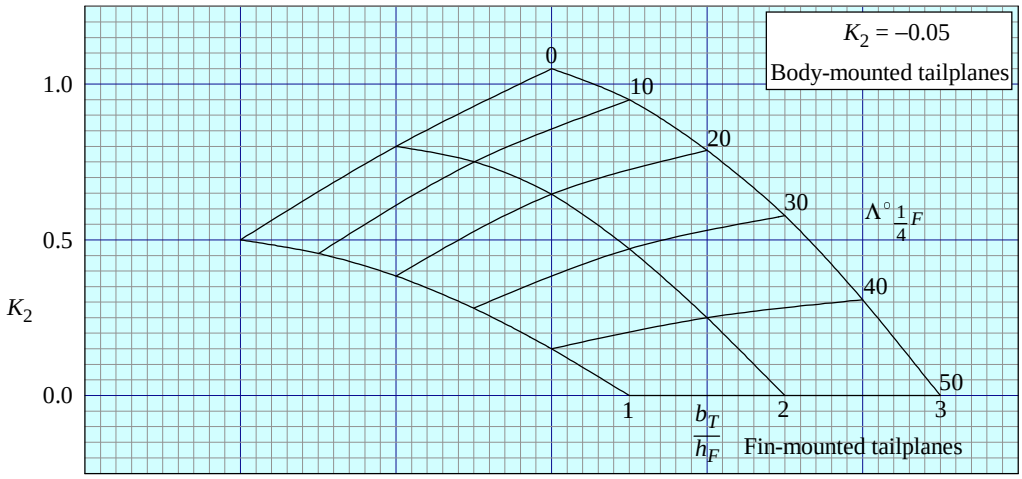

FIGURE 1b TAILPLANE INTERFERENCE PARAMETER K_2

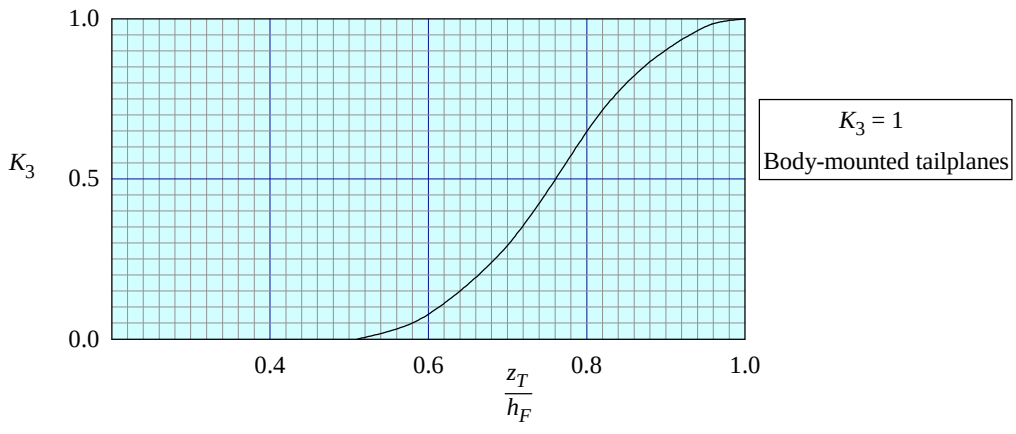

FIGURE 1c TAILPLANE INTERFERENCE PARAMETER K_3

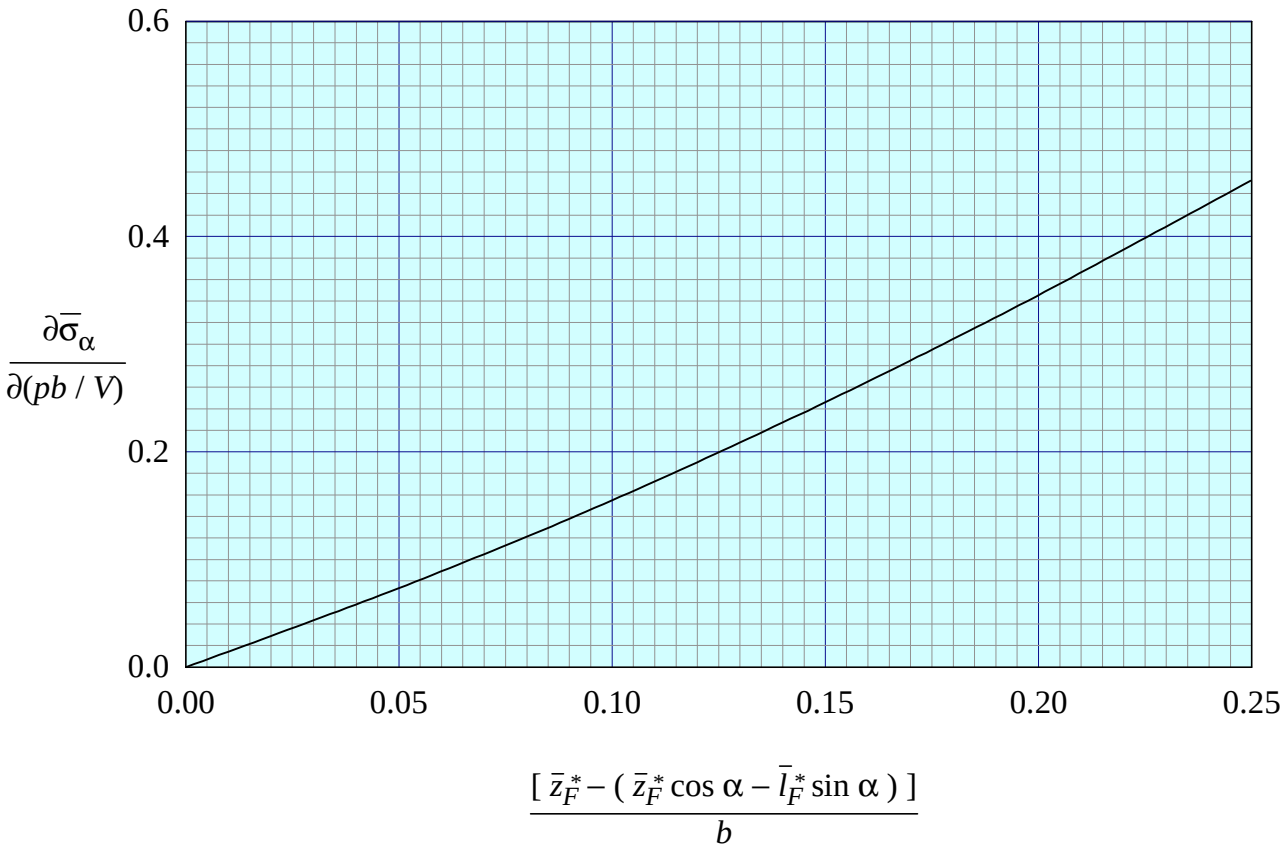

FIGURE 2 PARAMETER ALLOWING FOR EFFECTS OF ANGLE OF ATTACK AND BODY SIDEWASH

THE PREPARATION OF THIS DATA ITEM

The work on this particular Item was monitored and guided by the Aerodynamics Committee which first met in 1942 and now has the following membership:

Chairman

Mr H.C. Garner	–	Independent

Vice-Chairman

Mr P.K. Jones	–	British Aerospace, Manchester Division

Members

Mr D. Bonenfant	–	Aérospatiale, Toulouse, France.
Mr E.A. Boyd	–	Cranfield Institute of Technology
Mr K. Burgin	–	Southampton University
Mr E.C. Carter	–	Aircraft Research Association
Mr J.R.J. Dovey	–	British Aerospace, Warton Division
Dr J.W. Flower	–	Bristol University
Mr A. Hipp	–	British Aerospace, Stevenage-Bristol Division
Dr B.L. Hunt*	–	Northrop Corporation, Hawthorne, Calif., USA
Mr J. Kloos*	–	Saab-Scania, Linköping, Sweden
Mr J.R.C. Pedersen	–	Independent
Mr I.H. Rettie*	–	Boeing Aerospace Company, Seattle, Wash., USA
Mr F.W. Stanhope	–	Rolls-Royce Ltd, Derby
Mr H. Vogel	–	British Aerospace, Weybridge-Bristol Division
Mr J. Weir	–	Salford University.

* Corresponding Member

The member of staff who undertook the technical work involved in the initial assessment of the available information and the construction and subsequent development of the Item was

Mr R.W. Gilbey	–	Senior Engineer.